Appl. Phys. B (2015) 120:517–525
DOI 10.1007/s00340-015-6160-7

Applied Physics B
Lasers and Optics

CrossMark

Influence of heat treatment on characteristics of In_2O_3/Ag/MoO_3 multilayer films as transparent anode for optoelectronic applications

Mohsen Ghasemi Varnamkhasti[1,2] · Esmaeil Shahriari[1,2]

Received: 3 March 2015 / Accepted: 13 June 2015 / Published online: 27 June 2015
© Springer-Verlag Berlin Heidelberg 2015

Abstract In this study, In_2O_3/Ag/MoO_3 (IAM) nano-multilayer films are designed, and optimum thickness of each layer is calculated. These films were deposited by thermal evaporation technique and then annealed in air atmosphere at different temperatures for 1 h. The effects of annealing temperature on electrical, optical, and structural properties of the IAM system were investigated. The UV–visible–near-IR transmittance and reflectance spectra confirmed that the annealing temperature has significant influence on the electro-optical characteristics of IAM films. High-quality IAM films with a low sheet resistance of 8.2 (Ω/□) and the maximum optical transmittance of 85 % at 120 °C annealing temperature were obtained. The effect of heat treatment on surface roughness of the layers was also investigated. Figure-of-merit quantity showed that the IAM films annealed at 120 °C have the best performance. X-ray diffraction patterns showed that the crystallinity of the structures enhanced with increase in annealing temperature. Organic light-emitting diodes (OLEDs) were fabricated on IAM anodes. The current density–voltage–luminance (J–V–L) characteristic measurements show that the electroluminescence performances of OLED with IAM anode are improved compared with the conventional ITO-based device. The results indicate that the designed system is suitable for use as transparent conductive anode in optoelectronic devices.

1 Introduction

Transparent conducting oxides (TCOs) are important materials due to their special optical and electrical properties. These films have been widely used in various applications, including electrochromic devices [1], photocatalysts [2], storage-type cathode ray tubes [3], energy-efficient windows [4], organic solar cells [5, 6], flat panel displays (FPD) [7], gas sensors [8], and OLEDs [9]. TCO films have distinct characteristics such as low electrical resistivity, high transparency in visible region, and high absorption in the ultraviolet (UV) and infrared (IR) regions. Among the existing TCOs, doped oxide-based thin films such as ZnO, In_2O_3, and SnO_2 have been widely studied for several decades due to their conductivity and high transparency in the visible range [10–12]. However, advanced devices such as OLEDs and organic photovoltaic cells require new TCO films with lower electrical resistivity and higher optical transmittance in the visible region. Recent investigations show dielectric/metal/dielectric (D/M/D) multilayer structures [13–18]. In these structures, the electrical conductivity is improved by very thin metal films. Semiconductor or dielectric films are deposited on both sides of the metal layer to prevent reflection from the metal in the visible region for obtaining a selective transparency. It is also known that the properties of multilayer systems depend on various parameters. In order to obtain optimal characteristics, such as high transparency in visible wavelength region, high reflectance in near-IR region, and low sheet resistance, some parameters such as selection of materials, thickness of layers, deposition rate, substrate temperature, annealing

✉ Mohsen Ghasemi Varnamkhasti
mphdghasemi@gmail.com; ghasemi.mohsen@sci.sku.ac.ir

Esmaeil Shahriari
shahriari@sci.sku.ac.ir

1 Department of Physics, Faculty of Sciences, Shahrekord University, P.O. Box 115, Shahrekord, Iran

2 Nanotechnology Research Center, Shahrekord University, 8818634141 Shahrekord, Iran

temperature, and other deposition conditions must be optimized. Among the mentioned parameters, annealing temperature is one of the key factors influencing electrical, optical, and structural properties of multilayer systems. In this work, the proposed structure for transparent conductive electrode is In_2O_3/Ag/MoO_3 or IAM. In_2O_3 was chosen as the semiconductor layer because of its high refractive index, chemical stability, high transmittance in visible region, and excellent adhesion to substrates. Ag metal film has low electrical resistivity, and MoO_3 is a semiconductor oxide with high transparency, chemical and thermal stability, and high work function (5.3 eV) which can be used as suitable buffer layer between the anode and the organic materials in organic devices [19]. In addition, based on our knowledge, this multilayer structure system as transparent conductive anode has not been studied so far. After design and optimization of IAM multilayer system, we fabricated them using thermal evaporation technique. Then, the effects of heat treatment on their electrical, optical, and structural properties were investigated. Properties of IAM films were measured versus annealing temperature by analyzing electrical resistivity, X-ray diffraction (XRD), atomic force microscopy (AFM) images, optical transmittance, and reflectance for OLEDs applications. Optimized IAM multilayer film was used as an effective transparent anode in OLED devices. Finally, the current density–voltage–luminance (J–V–L) characteristics of OLED devices with IAM multilayer system as the anode were investigated.

2 Experimental details

Glass substrates were cleaned sequentially with acetone, isopropanol, ethanol, and dichloromethane in an ultrasonic cleaner for 10 min and then rinsed with de-ionized water and dried with a nitrogen flow. The multilayer systems were successively deposited without vacuum break using In_2O_3 (99.99 % purity), Ag powder (99.99 % purity), and MoO_3 (99.99 % purity) as source materials. Deposition of all films was performed at a pressure of 3×10^{-5} mbar in the vacuum chamber. The thickness of each layer was measured using a quartz crystal thickness monitor. During the deposition of the In_2O_3 (25 nm)/Ag (12 nm)/MoO_3(35 nm) multilayer system, the deposition rate of In_2O_3 and MoO_3 was 0.05 nm $s^{-1}$and Ag was 0.1 nm s^{-1}. The deposited films have been annealed in air at 60, 120, and 180 °C in steps of 60 °C for 1 h. The sheet resistance of multilayer films was measured by a four-point probe at room temperature. Electrical properties of the IAM films were investigated by Hall effect measurements. The crystal structure of IAM films annealed at different temperatures was characterized using XRD technique with a D8 Advanced Bruker X-ray diffractometer at room temperature, with monochromated Cu-Kα radiation system with wavelength 1.54 Å in the scan range of 2θ between 10° to 80° with a step size of 0.01 (2θ/s). Measurements were performed under beam-acceleration conditions of 40 kV/35 mA. The surface root-mean-square roughness was also determined using atomic force microscope (AFM-Ara Research Co.). Optical measurements of the samples were performed in the wavelength range from 300 to 2400 nm with a double-beam spectrophotometer (Shimadzu UV 3100) by recording the UV–visible optical transmission and near-IR reflection spectra of IAM thin films. The J–V–L characteristics of OLED devices were measured using a source-measure unit (Keithley, 2400) and JAZ Spectrometer (Ocean Optics). The electroluminescence measurements of our samples were performed under ambient conditions without any encapsulation.

3 Results and discussions

3.1 Design procedure

The design process for the IAM multilayer system was done using a Film Wizard® code. Optical transmittance and reflectance of the In_2O_3 (d_1 nm)/Ag (d_2 nm)/MoO_3 (d_3 nm) system for different values of d_1, d_2, and d_3 thicknesses were calculated in each step. Also, the sheet resistance of a multilayer system is very important for performance evaluation of transparent conductive coatings. Thus, theoretical sheet resistance of this system was calculated using the following equation [20, 21]:

$$R_{sh} = \frac{Z_0}{2}\left(\frac{1}{\sqrt{R}} - 1\right) \tag{1}$$

where R is the reflectance of infrared region, R_{sh} is sheet resistance, and $Z_0 = 377\ \Omega$ is the impedance of free space. We know that reflectance in infrared region is related to the electron concentration of films. According to the literature, the reflectance at 1700 nm (R_{1700}) can be applied as the criterion for the reflectance in infrared region [22]. Moreover, higher R_{1700} exhibits stronger reflecting in the near-infrared region. The figure of merit (F_{TC}) is an important index that exhibits briefly the relationship between electrical and optical properties of transparent conductive coatings. This quantity is defined by Haacke as the following equation [23]:

$$F_{TC} = \frac{T^{10}}{R_{sh}} \tag{2}$$

where T is the transmittance of films at 550-nm wavelength. Thickness of each layer was used as design parameter in this process to attain the desired values for figure of merit. Optimum thicknesses for In_2O_3, Ag, and MoO_3 layers were found to be 25, 12, and 35 nm, respectively. This

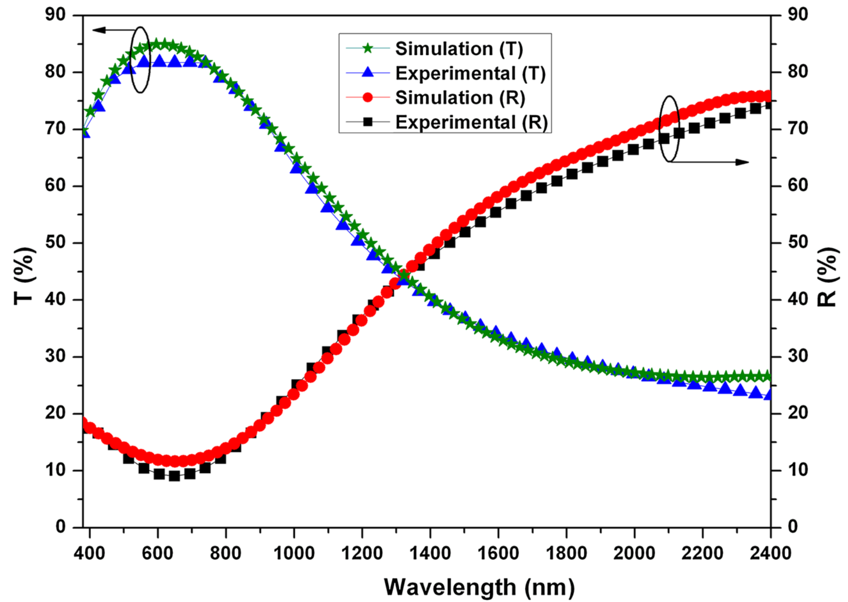

Fig. 1 Comparison of the experimental transmittance and reflectance spectra of In_2O_3 (25 nm)/Ag(12 nm)/MoO_3 (35 nm) with simulation results

designed three-layer structure was prepared as explained in the previous section. Figure 1 shows the simulated and measured optical transmittance and reflectance spectra of the In_2O_3 (25 nm)/Ag (12 nm)/MoO_3 (35 nm) multilayer system. Based on Eq. 1, the calculated theoretical sheet resistance for simulated IAM structure is 48.5 (Ω/□), while for fabricated sample it was found to be 49.3 (Ω/□), which indicates good agreement. As can be seen, the measured optical transmission and reflection are slightly lower than the simulated curve. Because, in the simulation process, the surface layers of In_2O_3, Ag, and MoO_3 are considered to be smooth, while the fabricated Ag, In_2O_3, and MoO_3 films have rough surfaces. Furthermore, surface plasmons in the rough Ag surface can be excited, and they allow incident light to be absorbed [24, 25]. Generally, the difference between the simulated and the measured transmittances pertains to the surface plasmons absorption at the Ag film. Although this multilayer system exhibits good performance, the effect of heat treatment has also been considered to improve optical and electrical characteristics.

3.2 Electrical properties

The conductivity of the multilayer system is essentially due to the metal film [26, 27]. A homogeneous continuous layer of Ag has low absorption and excellent electrical conductivity. The electrical behavior of Ag layers is attributed to transition from distinct islands of metal atoms to the formation of continuous layer [28]. According to the literature, the critical thickness of the Ag layer for the transition from separate islands to a continuous layer is usually between 10 and 20 nm [29]. In our research, the optimized thickness value of Ag layer in the design of IAM multilayer system is 12 nm, which falls well inside the mentioned range. Carrier concentration was measured using Hall effect. The Hall coefficient (R_H) was determined using the formula [30]:

$$R_H = \frac{V_H t}{I_x B_z} \tag{3}$$

where V_H is the Hall voltage measured, t is the thickness of the film, I_x is the current flowing through the film, and B_z is the magnetic field applied. The measured Hall coefficient (R_H) was used to calculate the carrier concentration (n) of the films by the equation:

$$n = \frac{1}{R_H e} \tag{4}$$

where e is the electron charge. The measured Hall coefficient (R_H) was also used to determine the Hall mobility using the following relation:

$$\mu = \frac{R_H}{\rho} \tag{5}$$

where ρ is the electrical resistivity. Carrier concentration and Hall mobility values are reported in Table 1. It should be noted that the sheet resistance is reciprocally proportional to the electron mobility and carrier concentration. The large volume fraction of voids will lead to small electron mobility and consequently large sheet resistance. When thickness is over the critical value, holes among the linked islands will be gradually filled and electron mobility will increase [21]. In addition, by filling of the voids in the layer, the average cross section is expanded and the current flow can be increased. Sheet resistance variations of the IAM multilayer films versus annealing temperature have been shown in Fig. 2. As can be seen, the sheet resistance

Table 1 Electrical, optical, and structural properties of IAM multilayer films at different annealing temperatures

Annealing temperature (°C)	Carrier concentration (10^{21} cm^{-3})	Hall mobility (cm^2/VS)	Grain size of Ag (nm)	Grain size of In_2O_3 (nm)	RMS roughness (nm)
As-deposited	7.48	2.3	–	–	0.67
60	8.57	4.1	15.1	25.7	1.01
120	13.81	7.6	19.2	35.8	1.27
180	0.16	37.7	–	45.6	5.39

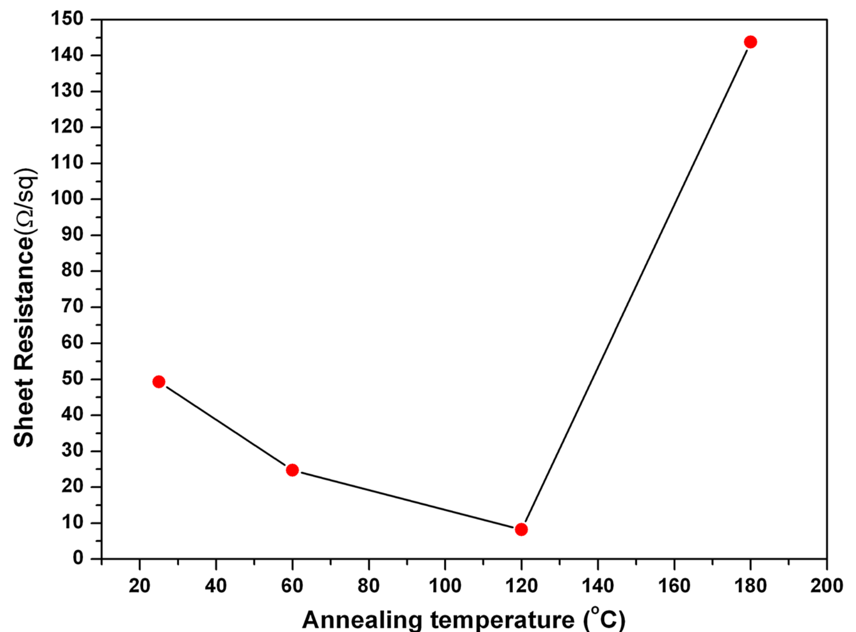

Fig. 2 Sheet resistance of the IAM multilayer films as a function of annealing temperature

is decreased slightly with increase in the annealing temperature from 49.3 (Ω/□) for as-deposited multilayer film to a minimum value of 8.2 (Ω/□) for annealing at 120 °C. The reduction in the sheet resistance pertains to the reduction in grain boundary scattering of the multilayer system in this range of temperatures [31]. The carrier mobility will increase when the reduction in the grain boundaries occurs, and therefore the sheet resistance of the IAM multilayer films is decreased. However, a significant increase in the sheet resistance can be observed with increase in the annealing temperature up to 180 °C. This behavior can be attributed to the intense interdiffusion of atoms at the Ag/MoO_3 and In_2O_3/Ag interfaces. In other words, oxygen atoms diffuse through Ag layers with the annealing in air at higher temperature, which results in oxidation of the metal layer. Therefore, at higher temperature, the sheet resistance increases in the films.

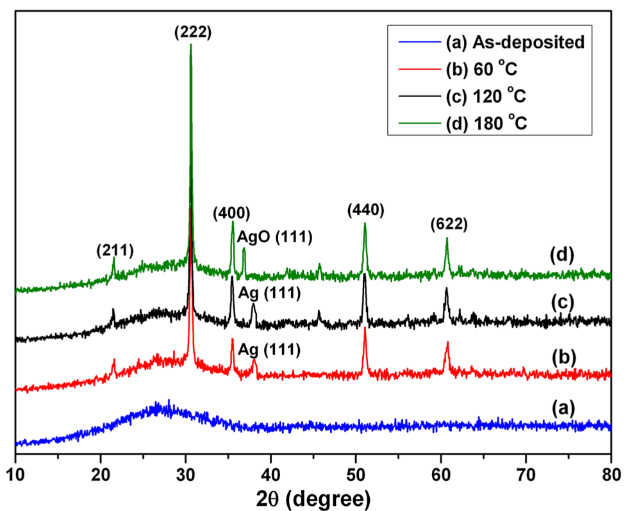

Fig. 3 XRD patterns of IAM multilayer films annealed at various temperatures

3.3 Structural properties

In order to study the influence of annealing temperature on the structural characteristics of the IAM multilayer system, the X-ray diffraction (XRD) measurements were performed. In Fig. 3, the XRD patterns of IAM films are

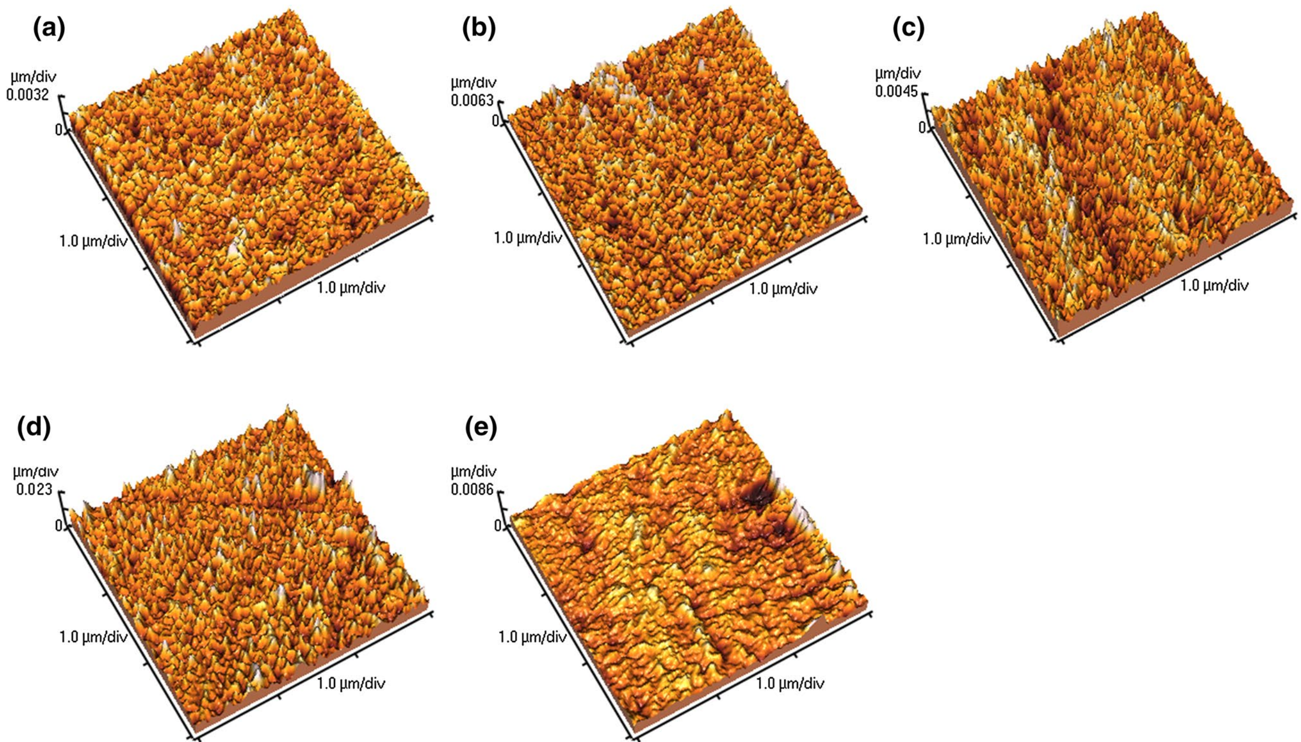

Fig. 4 AFM images of the IAM films at different annealing temperature. **a** As-deposited, **b** 60 °C, **c** 120 °C, **d** 180 °C and **e** ITO

shown before and after annealing. It can be seen that only one unimportant shoulder appears in the 2θ between 20° and 30° before annealing. This feature shows an amorphous structure for the as-deposited IAM multilayer system. The crystallinity of the same film was improved after heat treatment. The annealed film pattern matches with reference peaks of body-centered cubic (bcc) In_2O_3. In particular, the line at $2\theta = 30.5°$ corresponds to the reflection from the (222) plane. The other peaks are due to the reflection from the (211), (400), (440), and (622) planes in In_2O_3 film. We have used full width at half maximum (FWHM) value of the strongest XRD line at $2\theta = 30.5°$ corresponding to the reflection from the (222) plane to estimate the grain size of In_2O_3. The diffraction peak at $2\theta = 38.2°$ is related to (111) Ag crystal orientation. The peak's intensity rises with increase in the annealing temperature. Also, by increasing annealing temperature up to 180 °C, the Ago peak (111) at $2\theta = 36.9°$ appeared which indicates the Ag layer is completely oxidized. None of the patterns exhibited any characteristic peaks of MoO_3, which means that the MoO_3 layer was amorphous in the IAM multilayer system. Since the grain boundary reduces the carrier mobility and consequently increases the sheet resistance, the effect of annealing temperature on grain size of Ag in the IAM multilayer films was also investigated. The grain size (*D*) was calculated using the Scherrer formula [32]:

$$D = \frac{0.9\lambda}{B\cos\theta} \quad (6)$$

Here, $\lambda = 1.54056$ Å and θ is the Bragg diffraction angle of the XRD peak and B is the full width at half maximum (FWHM). The average grain sizes of Ag and In_2O_3 in the annealed films at various annealing temperatures are calculated and presented in Table 1. As the annealing temperature is increased, the grain size is increased and, as a result, the crystallinity of the films is improved.

AFM images of the IAM multilayer films annealed at different temperature and commercial available ITO film are shown in Fig. 4a–e. The root-mean-square (RMS) surface roughness of IAM multilayer films is listed in Table 1 and for ITO film is 2.65 nm. The RMS roughness initially increased slightly when the annealing temperature increased from 25 to 120 °C. However, the roughness increased sharply with further increase in the annealing temperature. It is found that IAM films annealed at lower temperatures have a relatively smooth surface with RMS roughness less than 1.5 nm, which is appropriate for efficient OLED devices. For an anode with a high RMS roughness, the hole-injection process is weak. The localized high electric fields induced by the surface roughness of the layer can create an unexpected current flow leading to a dark spot formation and a reduction in device luminous intensity or a short device operation lifetime [33].

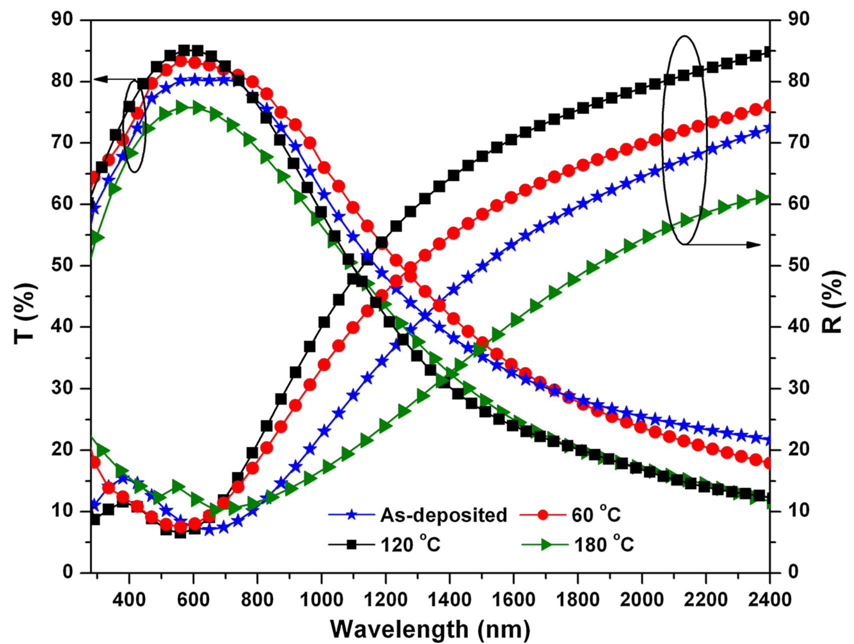

Fig. 5 Optical transmission and reflection spectra of IAM films at various annealing temperatures

3.4 Optical properties

Figure 5 exhibits the optical transmittance and reflectance spectra of the IAM multilayer films deposited on glass substrates as a function of the annealing temperature. It can be observed that the films are transparent in the visible region and are highly reflective in the infrared region. Also, the optical transmission of IAM multilayer films improves with increase in annealing temperature up to 120 °C and decreases with further increase. The post-deposition annealing of multilayer process improves crystallization and decreases the density of crystalline defects, allowing one to obtain films that are more transparent and conductive [34]. The optical transmittance decreases by further increasing annealing temperature up to 180 °C. It seems that this result pertains to surface roughening of Ag layer during annealing at high temperatures and diffusion of Ag atoms into other layers which causes more scattering of the incident light and so reduction in the transmittance in IAM films. The reflectance spectra of the multilayer systems are presented in Fig. 5. The increase in the reflectance in the near-infrared region is basically due to the interaction of free electrons in the multilayer system with the incident radiation. The results (Table 1) indicated that the highest carrier concentration was obtained for the annealed film at 120 °C. Thus, this layer has the highest reflectance in the IR region. A plot of the figure of merit as a function of annealing temperature is shown in Fig. 6. It can be seen that with increase in the annealing temperature, the F_{TC} value increases and the maximum F_{TC} value of the IAM multilayer system can be obtained at 120 °C annealing temperature. However, further increase in the annealing

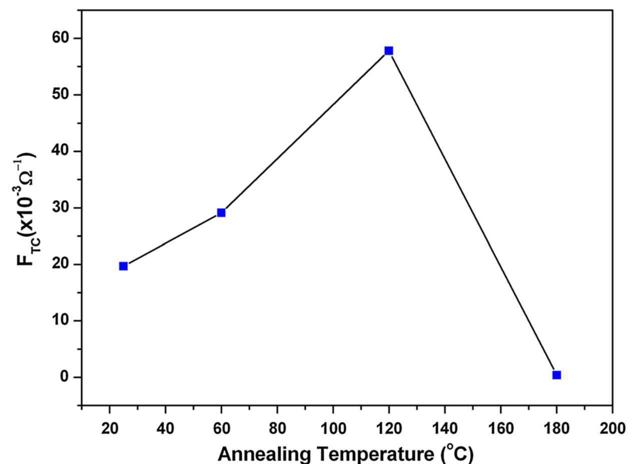

Fig. 6 Figure-of-merit values of the IAM films as a function of annealing temperature

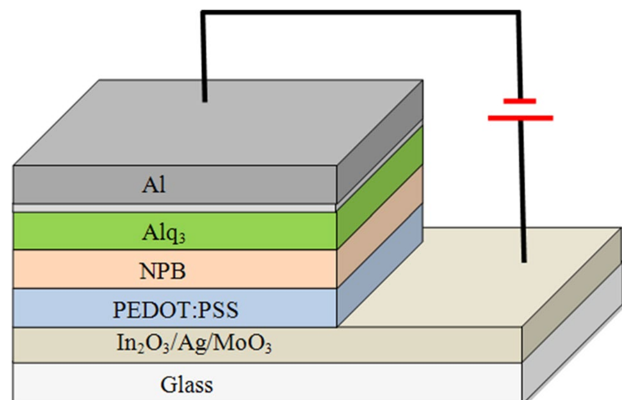

Fig. 7 Schematic structure of the organic light-emitting diode under study

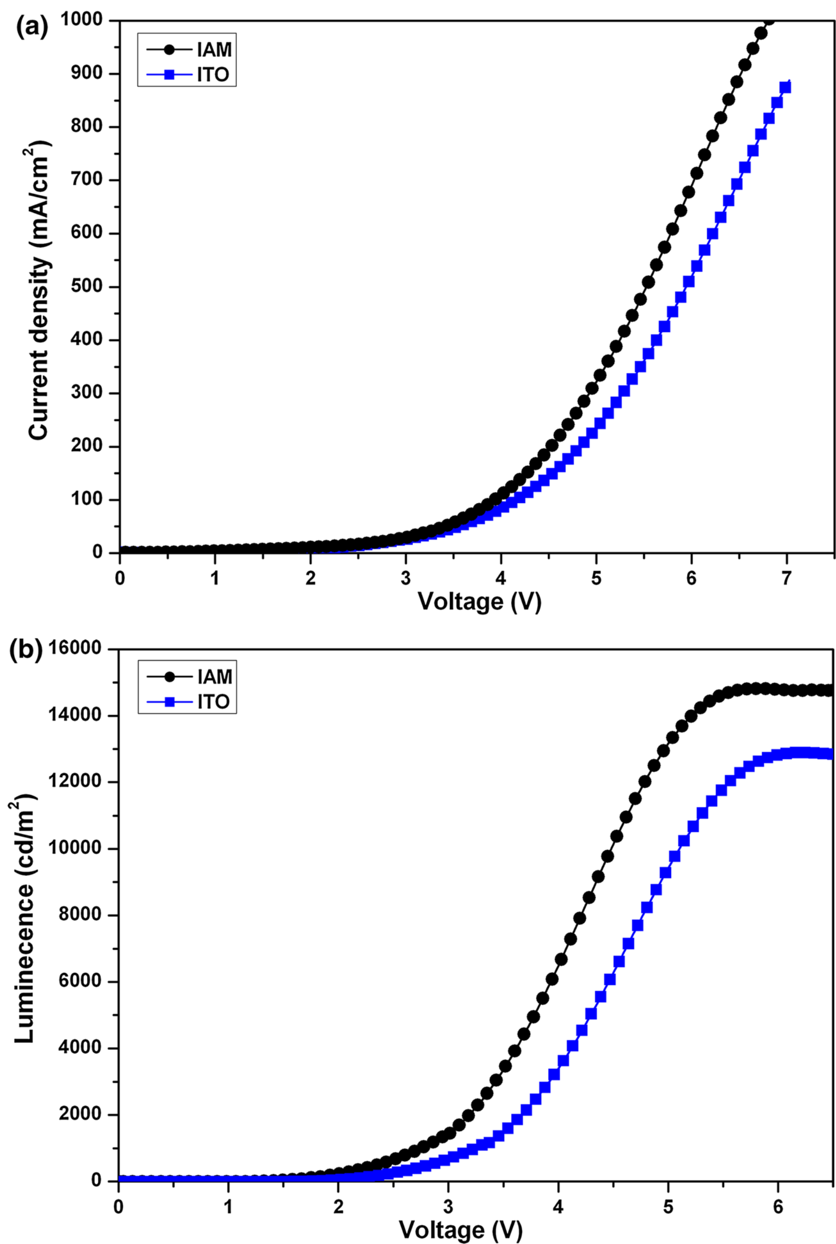

Fig. 8 **a** J–V and **b** L–V characteristics of OLEDs with IAM and ITO anodes

temperature leads to a decrease in F_{TC} value. Higher F_{TC} represents a better quality of IAM multilayer system; therefore, the IAM multilayer films annealed at 120 °C have a suitable structure for use in optoelectronic devices.

3.5 Organic light-emitting-diode fabrication

In order to examine and demonstrate the performance of the fabricated IAM films, organic light-emitting diodes with IAM/PEDOT:PSS(35 nm)/NPB(45 nm)/Alq3(45 nm)/LiF (0.7 nm)/Al (140 nm) structure were fabricated. PEDOT:PSS [poly(3, 4-ethylenedioxythiophene)-poly(styrenesulfonate)] as a hole-injection layer was deposited by spin coating on the anode. NPB [*N*,*N*′-di(naphthalene-1-yl)–*N*,*N*′-diphenyl-benzidine] as a hole transport layer and Alq_3 [tris(8-hydroxyquinoline) aluminum] as an emitting and electron transport layer with 45 nm thickness at a rate of 0.1 Å/s were successively deposited. Finally, 0.7-nm-thick LiF layer as cathode buffer layer and 140-nm Al as a metal cathode were evaporated to complete the device fabrication. The active area for the device is 3×5 mm^2. Schematic structure of the OLED fabricated on the IAM electrode is shown in Fig. 7. In the structure of OLEDs, optimized IAM multilayer system and LiF/Al were used as anode and top cathode, respectively. For comparison, an identical OLED was deposited on the conventional ITO-coated glass with a sheet resistance of 15 (Ω/□) simultaneously under the same growth conditions.

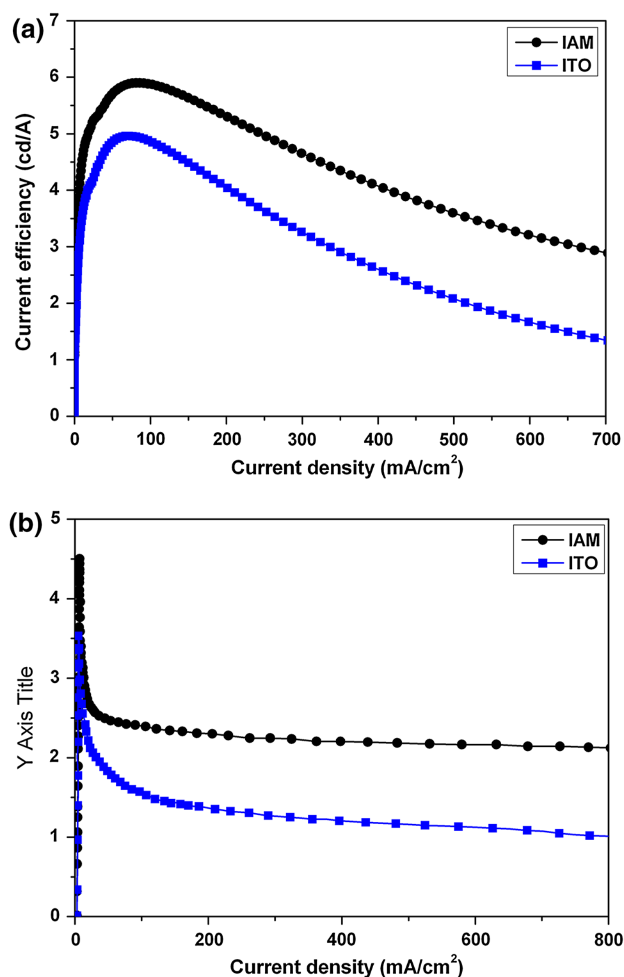

Fig. 9 **a** Current efficiency–current density and **b** Power efficiency–current density characteristics of IAM-based OLED and ITO-based OLED

Figure 8a, b shows the current density–voltage–luminance (J–V–L) characteristics of OLEDs with bare ITO and IAM anodes. It can be seen that the turn-on voltage shifts toward a lower voltage, and luminance intensity of OLED prepared on IAM anode is higher than the device with ITO anode for the same applied voltage. This behavior is due to more injection of holes, and hence the turn-on voltage is decreased and current density is increased. The maximum luminance of device with IAM anode is 14,818 cd/m^2 at a driving voltage of 5.8 V. The current and power efficiencies versus current density of OLED devices are shown in Fig. 9a, b. The OLED devices with IAM anode exhibits higher current and power efficiencies with respect to the ITO-based device in the whole experimental range, especially in the high current density region. The maximum current and power efficiency values of OLED devices with IAM anode are 5.9 (cd/A) and 4.53 (lm/W), respectively, whereas these values for ITO-based OLED are 4.93 (cd/A) and 3.52 (lm/W), respectively. As a consequence, the highest current efficiency and power efficiency are improved 19.6 and 28.6 %, respectively, compared with the ITO anode. It is known that the current efficiency is determined by the balance of holes and electrons [35]. Thus, improvement in performance of the IAM-based OLED device can be attributed to an improved IAM/hole transport layer interface quality, increased hole injection, and a more balanced hole–electron current. It is a well-known fact that the formation of ohmic contact is important for charge carrier injection in OLED devices. In general, the carrier injection for the OLEDs is subject to the work function and the electrical resistivity of the anode material [36]. The sheet resistance of optimized IAM electrode was 8.2 (Ω/□) which is lower than the ITO anode (15 (Ω/□)). Besides, the work function of multilayer electrode is derived from the upper layer [20]. The work function of MoO_3 in the IAM anode is 5.3 eV, which has good band structure matching with the highest occupied molecular orbital (HOMO) level of PEDOT:PSS (5.2 eV), while the work function of ITO is 4.8 eV. It should also be noted that the low work function of IAM anode helps reduce the energy barriers at the anode–organic interface, facilitate the transportation of the charged carriers, confine the opposite charges inside the emission layer, and consequently improve the power efficiency of the device [37]. Furthermore, the surface electronic and morphological properties at anode–organic interfaces control the hole injection of OLED devices, and hence, these properties play an important role in determining the devices performance [37]. RMS roughness values for the commercial ITO films and the optimized IAM multilayer system is 2.65 and 1.27 nm, respectively. The localized high electric fields induced by the rough surface can also lead to a non-uniform current flow causing the dark spot formation and a decrease in device luminous intensity. Thus, the device based on IAM anode shows higher light-emitting efficiency than that with ITO anode because of higher work function, lower resistivity, and lower RMS roughness of IAM film.

4 Conclusion

The In_2O_3/Ag/MoO_3 (IAM) nano-multilayer films as a transparent conductive coating with high transparency in visible region and high electrical conductivity were designed and fabricated on glass substrate. Then, the samples were annealed in air at different temperatures from 60 to 180 °C for 1 h to investigate the effects of heat treatment on the electrical, optical, and structural properties of the samples. The figure of merit shows that the optimum annealing temperature for obtaining best performance of IAM films is 120 °C. The XRD results showed that the

crystallinity of the samples was improved by annealing process. The AFM images indicated that the RMS roughness of IAM films can be affected by annealing process. High-quality films with low sheet resistance [8.2 (Ω/□)], high transmittance in visible region (about 85 %), and surface roughness (RMS = 1.27 nm) were achieved in optimum temperature. We demonstrated that the IAM structure can be used as an effective transparent anode in organic light-emitting diodes. OLEDs with structure of anode/PEDOT:PSS/NPB/Alq_3/LiF/Al were fabricated on optimized IAM films as anode and commercially available ITO anode for evaluation and comparison. It was found that electroluminescence characteristics of organic diodes with IAM anode are better than the ITO-based OLEDs.

Acknowledgments The authors would like to thank the Nanotechnology Research Center of Shahrekord University for their Support.

Compliance with ethical standards

Conflict of interest The authors state that there are no conflicts of interest.

References

1. A. Subrahmanyam, A. Karuppasamy, Sol. Energy Mater. Sol. Cells **91**, 266 (2007)
2. K. Muthu Karuppasamy, A. Subrahmanyam, Sol. Energy Mater. Sol. Cells **92**, 1322 (2008)
3. M.J. Alam, D.C. Cameron, Thin Solid Films **377**, 455 (2000)
4. A.M. Al-Shukri, Desalination **209**, 290 (2007)
5. F.C. Krebs, Sol. Energy Mater. Sol. Cells **93**, 394 (2009)
6. F.C. Krebs, M. Jorgensen, Sol. Energy Mater. Sol. Cells **119**, 73 (2013)
7. B.H. Lee, I.G. Kim, S.W. Cho, S.H. Lee, Thin Solid Films **302**, 25 (1997)
8. B.K. Min, S.D. Choi, Sens. Actuators B **98**, 239 (2004)
9. E. Nam, Y.H. Kang, D. Jung, Y.S. Kim, Thin Solid Films **518**, 6245 (2010)
10. S.K. Poznyak, A.N. Golubev, A.I. Kulak, Science **454**, 396 (2000)
11. M.G. Varnamkhasti, H.R. Fallah, M. Zadsar, Vacuum **86**, 871 (2012)
12. M. Zadsar, H.R. Fallah, M.H. Mahmoodzadeh, A. Hassanzadeh, M.G. Varnamkhasti, Mater. Sci. Semicond. Process. **15**, 432 (2012)
13. D. Kim, Appl. Surf. Sci. **256**, 1774 (2010)
14. J. Kulczyk-Malecka, P.J. Kelly, G. West, G.C.B. Clarke, J.A. Ridealgh, K.P. Almtoft, A.L. Greer, Z.H. Barber, Acta Mater. **66**, 396 (2014)
15. Z. Yu, J. Leng, W. Xue, T. Zhang, Y. Jiang, J. Zhang, D. Zhang, Appl. Surf. Sci. **258**, 2270 (2012)
16. H.K. Park, J.W. Kang, S.I. Na, D.Y. Kim, H.K. Kim, Sol. Energy Mater. Sol. Cells **93**, 1994 (2009)
17. C. Guillen, J. Herrero, Phys. Status Solidi A. **206**, 1531 (2009)
18. D.R. Sahu, J.L. Huang, Thin Solid Films **516**, 208 (2007)
19. Y. Kanai, T. Matsushima, H. Murata, Thin Solid Films **518**, 537 (2009)
20. G. Leftheriotis, S. Papaefthimiou, P. Yianoulis, Solid State Ion. **136**, 655 (2000)
21. P. Zhao, W. Su, R. Wang, X. Xu, F. Zhang, Phys. E **41**, 387 (2009)
22. X. Liu, X. Cai, J. Mao, Thin Solid Films **441**, 200 (2003)
23. G. Haacke, J. Appl. Phys. **47**, 4086 (1976)
24. S.M. Lee, C.S. Choi, K.C. Choi, H.C. Lee, Org. Electron. **13**(9), 1654 (2012)
25. H. Kermani, H.R. Fallah, M. Hajimahmoodzadeh, Phys. E **47**, 303 (2013)
26. D.R. Sahu, J.L. Huang, Thin Solid Films **515**, 876 (2006)
27. L. Cattin, M. Morsli, F. Dahou, S.Y. Abe, A. Khelil, J.C. Bernede, Thin Solid Films **518**, 4560 (2010)
28. J.H. Park, K.J. Ahn, K.I. Park, S.I. Na, H.K. Kim, J. Appl. Phys. D. **43**, 115101 (2010)
29. J.A. Jeong, H.K. Kim, M.S. Yi, Appl. Phys. Lett. **93**, 033301 (2008)
30. S. Bhagwat, R.P. Howson, Surf. Coat. Technol. **111**, 163 (1999)
31. M. Neghabi, A. Behjat, S.M.B. Ghorashi, S.M.A. Salehi, Thin Solid Films **519**, 5662 (2011)
32. E. Gagaoudakis, M. Bender, E. Douloufakis, N. Katsarakis, E. Natasakou, V. Cimalla, G. Kiriakidis, Sensor. Actuators B **80**, 155 (2001)
33. G. Liu, J.B. Kerr, S. Johnson, Synth. Met. **144**, 1 (2004)
34. C. Guillen, J. Herrero, Thin Solid Films **520**, 1 (2011)
35. L. Cattin, F. Dahou, Y. Lare, M. Morsli, R. Tricot, S. Houari, A. Mokrani, K. Jondo, A. Khelil, K. Napo, J.C. Bernede, J. Appl. Phys. **105**, 034507 (2009)
36. F. Li, Y. Zhang, C. Wu, Z. Lin, B. Zhang, T. Guo, Vacuum **86**(12), 1895 (2012)
37. Z. Li, Z. Rick Li, H. Meng, *Organic Light-Emitting Materials and Devices* (CRC Taylor and Francis, New York, 2007)